Combustion Science and Technology
Publication details, including instructions for authors and subscription information:
http://www.informaworld.com/smpp/title~content=t713456315

Combustion and Conversion Efficiency of Nanoaluminum-Water Mixtures

Grant A. Risha [a]; Justin L. Sabourin [b]; Vigor Yang [b]; Richard A. Yetter [b]; Steven F. Son [c]; Bryce C. Tappan [d]
[a] The Pennsylvania State University, Altoona College, Altoona, PA, USA [b] The Pennsylvania State University, University Park, PA, USA [c] Purdue University, West Lafayette, IN, USA [d] Los Alamos National Laboratory, Los Alamos, New Mexico, USA

Online Publication Date: 01 December 2008

To cite this Article Risha, Grant A., Sabourin, Justin L., Yang, Vigor, Yetter, Richard A., Son, Steven F. and Tappan, Bryce C.(2008)'Combustion and Conversion Efficiency of Nanoaluminum-Water Mixtures',Combustion Science and Technology,180:12,2127 — 2142

To link to this Article: DOI: 10.1080/00102200802414873

URL: http://dx.doi.org/10.1080/00102200802414873

Combust. Sci. and Tech., 180: 2127–2142, 2008

ISSN: 0010-2202 print/1563-521X online
DOI: 10.1080/00102200802414873

Taylor & Francis
Taylor & Francis Group

COMBUSTION AND CONVERSION EFFICIENCY OF NANOALUMINUM-WATER MIXTURES

Grant A. Risha[1], Justin L. Sabourin[2], Vigor Yang[2], Richard A. Yetter[2], Steven F. Son[3], and Bryce C. Tappan[4]

[1]*The Pennsylvania State University, Altoona College, Altoona, PA, USA*
[2]*The Pennsylvania State University, University Park, PA, USA*
[3]*Purdue University, West Lafayette, IN, USA*
[4]*Los Alamos National Laboratory, Los Alamos, New Mexico, USA*

An experimental investigation on the combustion behavior and conversion efficiency of nanoaluminum and liquid water mixtures was conducted. Burning rates and chemical efficiency of aluminum-water and aluminum-water-poly(acrylamide-co-acrylic acid) mixtures were quantified as a function of pressure (from 0.12 to 15 MPa), nominal aluminum particle size (for diameters of 38, 50, 80, and 130 nm), and overall equivalence ratios ($0.67 < \phi < 1.0$) under well-controlled conditions. Chemical efficiencies were found to range from 27 to 99% depending upon particle size and sample preparation. Burning rates increased significantly with decreased particle size attaining rates as high as 8 cm/s for the 38 nm diameter particles above approximately 4 MPa. Burning rate pressure exponents of 0.47, 0.27, and 0.31 were determined for the 38, 80, and 130 nm diameter particle mixtures, respectively. Also, mixture packing density varied with particle size due to interstitial spacing, and was determined to affect the burning rates at high pressure due to inert gas dilution. The presence of approximately 3% (by mass) poly(acrylamide-co-acrylic acid) gelling agent to the nAl/H_2O mixtures had a small, and for many conditions, negligible effect on the combustion behavior.

Keywords: Aluminum; Burning rate; Combustion; Efficiency; Nanoparticles; Water

INTRODUCTION

Thermodynamically, many metals react with liquid water to produce exothermic reactions (see for example, Greiner, 1962; Rasor, 1942; Greiner, 1960; Foote et al., 1996, Ingenito and Bruno, 2004 for studies on the reaction of aluminum with

This work was sponsored by the U.S. Army Research Office under the Multi-University Research Initiative under Contract No. W911NF-04-1-0178 and the Office of Naval Research (ONR) under Grant No. N00014-03-1-0595. The support and encouragement provided by Drs. David Mann, Kevin L. McNesby, and Gabriel Roy are gratefully acknowledged. S.F.S. and B.C.T. are supported by the Joint Munitions Program (DoD/DOE) at the Los Alamos National Laboratory (LANL), which is operated by the University of California for the U.S. Department of Energy under the contract W-7405-ENG-36. The authors would like to thank personnel at LANL, specifically Mr. Eric Sanders for supplying the 38-nm aluminum particles and Dr. Joseph T. Mang for SAS and BET data for the 80-nm particles.

Address correspondence to Prof. Grant Risha, Division of Business and Engineering, Altoona, PA 16610. E-mail: gar108@psu.edu

liquid water). Reactions between Al and water or other oxidizers occur in many explosive and propulsion systems. Numerous fundamental studies on aluminum with oxygen or air exist in the literature (e.g., Bucher et al., 1998; Glassman, 1996; Goroshin et al., 1996; Williams, 1997, 1985; Yetter and Dryer, 2001) but few have been devoted to the Al-H_2O reaction (Basilev et al., 1970; Ivanov et al., 1994, 1995, 2000; Lee, 1993; Miller and Herr, 2004; Tao et al., 1990) and even less using nanosized aluminum (Il'in et al., 2001; Parr et al., 1999; Risha et al., 2005, 2006, 2007; Shafirovich et al., 2006; Trunov et al., 2005).

Micron-sized Al particles demand long combustion times and require high ignition temperatures. The possibility of increasing the reactivity of metal particulates, thereby lowering ignition temperatures and shortening reaction times could greatly enhance existing uses of metal powders as well as to produce new methods for their use in combustion systems. Therefore, nanosized particles are desirable since they offer shortened ignition delay, decreased burn times, more complete combustion, higher specific surface area, and the ability to act as gelling agents for liquids, replacing inert or low energy gelling agents. Unfortunately, fundamental studies on the combustion (reaction) of a single nanoparticle are difficult, and consequently, mixtures of nanoparticles with oxidizers are studied.

In the present paper, we study the reaction of nanoaluminum particles (nAl) with liquid water in quasi-homogeneous mixtures in order to better understand the combustion process of a simple two component heterogeneous system. From a practical point of view, this reaction is also being considered as a potential approach to solid hydrogen storage because of the significant amount of hydrogen produced from the reaction (Smith, 1972). Hydrogen can be produced rapidly and at high temperatures from this reaction, provoking consideration of aluminum-water combustion for propulsion applications (Ingenito and Bruno, 2004).

From a fundamental perspective, the combustion process is also very interesting because the adiabatic flame temperature is close to the vaporization temperature of aluminum, and consequently, aluminum may either react in the vapor phase or condensed phase depending upon the pressure and initial temperature of the mixture. From equilibrium calculations, the exothermicity of the water reaction with aluminum at ambient temperature produces an adiabatic flame temperature that exceeds the vaporization temperature only for pressures below 1.5 atm. However, as the pressure is increased, the vaporization temperature of aluminum exceeds the adiabatic flame temperature for liquid water and Al system. At elevated pressures, the combustion process would be predicted to occur at the particle surface typical of a heterogeneous surface reaction, much like occurs in boron or carbon particle combustion.

Ivanov et al. (1994, 2000) investigated the effect of pressure on ultrafine aluminum metal powders (UFP) in a mixture of water in the presence of a thickening agent, polyacrylamide (3%). The specific surface area of their particles ranged from 5–50 m^2/g. In their experiment, they mixed UFP aluminum with distilled water and added the thickening agent at equivalence ratios of 0.67 and 1.0. They reported that the mixture would not ignite without including the polyacrylamide thickening agent in the mixture. The mixture was filled into 10-mm tubes and ignited with an electrical coil inside of a constant pressure vessel with argon as the atmospheric gas. Mixture compositions ranged from 40 to 55% (by mass). At the maximum test pressure of 7 MPa, the maximum burning rate of the mixture was found to be approximately 1.5 cm/s. Ivanov et al. did not

report packing densities of each sample; therefore, mass-burning rates could not be determined. Shafirovich et al. (2006) investigated the combustion behavior of 80 nm nAl-water mixtures, also using a polyacrylamide gelling agent. They found that 80 nm nAl-H_2O mixtures yielded a combustion efficiency of $\sim$50%.

In a previous study by the present authors (Risha et al., 2007), the combustion of nAl and liquid water was investigated without the use of any additional gelling agent. Steady-state burning rates were obtained at room temperature ($\sim$25°C) using a windowed vessel for a pressure range of 0.1 to 4.2 MPa in an argon atmosphere with particles having a nominal diameter of 38 nm. The effects of particle diameter (50, 80, and 130 nm) and overall mixture equivalence ratio ($0.5 < \phi < 1.25$) on the burning rate were also studied at a pressure of 3.65 MPa. In this study, our previous research was extended to higher pressures ($\sim$15 MPa) to further characterize the burning process of nAl-H_2O mixtures, and in particular, to assess the role of the gelling agent used by previous investigators on the combustion process. The burning rate pressure dependence of larger 80 and 130 nm Al particles were also determined. In addition, experiments were developed to study the efficiency of the reaction by measuring the hydrogen produced under constant volume conditions. Combustion efficiency data were obtained for several nominal particle diameters (38, 50, 80, and 130 nm), equivalence ratios of 0.67 and 1, and pressures ranging from atmospheric to approximately 15 MPa.

EXPERIMENT

Two experiments were used in this investigation. The first was an optical pressure vessel (Figure 1a), which was used to determine the steady-state linear and mass burning rates under near constant pressure conditions. The second, a constant volume closed chamber (Figure 1b), was used to contain the combustion products of the mixture and measure the amount of gaseous hydrogen produced from the Al-H_2O reaction at various initial pressures. From the hydrogen produced, chemical conversion efficiencies were determined.

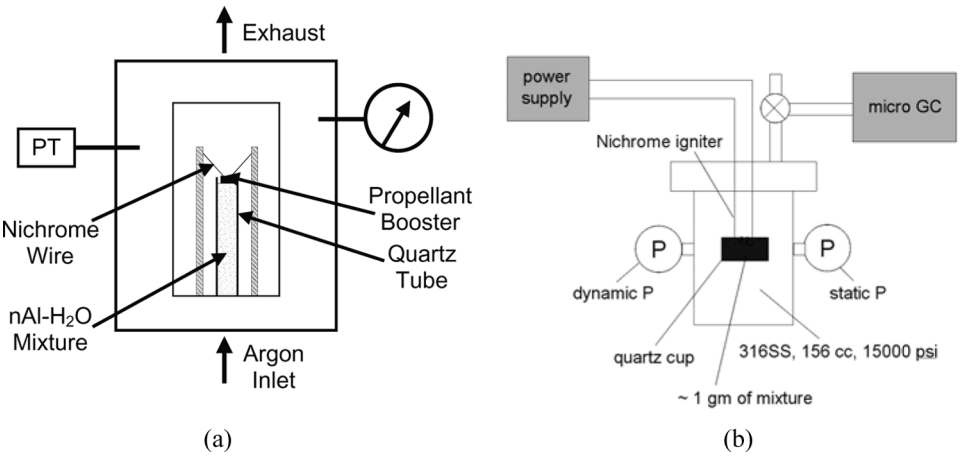

Figure 1 (a) Schematic diagram of windowed pressure vessel, (b) closed bomb efficiency testing schematic.

The 38 nm nAl particles used in the present study were supplied from Technanogy with an active aluminum content of 54.3% (by weight). The 50, 80, and 130-nm particles were supplied by Nanotechnologies, Inc. (Table 1). Particle densities, inclusive of the oxide coating, were measured using a pycnometer and had values near 3 g/cm^3 (compared to bulk Al of 2.7 g/cm^3). The nAl particles were mixed manually in small batches with distilled water (oxidizer) in a sealed plastic bag (Risha et al., 2007).

For tests including the poly(acrylamide-co-acrylic acid) or "Poly-A" (Sigma-Aldrich, MW = 5,000,000, CAS Number 009003069), the oxidizer preparation was slightly different. Three weight percent of Poly-A was added to the distilled water and well mixed prior to introducing the nAl. After sufficient mixing, the water became gel-like. The active aluminum content corresponding to the respective nAl particles was balanced with the water content (97%, by wt) in the oxidizer as specified by the desired stoichiometry and mixed with the aluminum in the exact same manner. The sample was loaded in the vessel immediately after packing to avoid any loss through vaporization or slow, low temperature reactions.

The burning rates of nAl mixtures with liquid water were obtained using the optical pressure vessel. The chamber, constructed from 316 stainless steel, is equipped with four optical viewing ports each having a 15.2×2.54 cm field of view. The 61 cm long chamber has an inner diameter of 22 cm and a total free volume of 23 liters to minimize the pressure variation caused by the generation of gaseous combustion products during an experiment. The optical chamber was brought to the desired initial pressure using argon as the pressurant gas by regulating the inlet and exhaust valves. The continuous purge of argon kept the product gases free from the viewing area. The base plate has six feedthrough ports to provide pathways into the chamber for electrical-signal and gas lines. One of the optical viewing ports was backlit using an optical diffuser. The opposite viewing port of the diffuser was used for real-time recording of the burning process with a digital video camera. The sample holders used to view the burning process were 10-mm O.D. (8-mm I.D.) quartz tubes ($\sim$75mm in length), in which the nAl-liquid water samples were manually packed using a metal plunger.

The instantaneous pressure was monitored using a Setra 206 pressure transducer. Ignition was obtained by resistance-heating of a double base booster propellant (NOSOL 363) with a nichrome wire that was threaded through the propellant. A data acquisition system (Nicolet Genesis) was used to record the pressure

Table 1 Characteristics of aluminum particles

Particle diameter [nm]	Oxide layer thickness [nm]	Active aluminum content [%]	Particle density[c] [g/cm^3]	Surface area [m^2/g]
38[a]	3.1	54.3	3.205	54.1
50[b]	2.1	68.0	3.008	41.2
80[b]	1.6	84.0	–	25.8
80[b]	1.9	81.0	3.076	26.5
80[b]	2.7	74.0	–	26.1
130[b]	2.2	84.0	–	16.5

[a]Manufactured by Technanogy, LLC.
[b]Manufactured by Nanotechnologies.
[c]Measured using a pycnometer.

transducer output at a sampling rate of 1000 Hz. The position and time of the regressing luminous front were monitored using the digital video recorder. From these data, the burning rate was determined using the curve fit of position vs. time data.

The packing density of the samples varies with particle size and overall equivalence ratio (Risha et al., 2007). For a given particle size and mixture ratio, the linear burning rate was found to vary with packing density as shown in Figure 2, although the mass-burning rate is relatively constant. The linear burning rate decreased by nearly 51% for a packing density increase of ~32%, whereas the mass burning rate per unit area changed less than 10–12%, which is within the scatter of the data. Therefore, mass-burning rate per unit area is also reported to account for any packing density variation.

A closed bomb chamber (capable of pressures as high as 35 MPa) coupled with gas chromatography was used to determine the hydrogen produced from the reaction between nAl and water. The chamber was constructed from 316 stainless steel with a free volume of 156 cm^3. A PCB fast-response sensor (111A22) and a static Setra 206 diaphragm transducer were used to monitor the pressure in the vessel. The instantaneous pressure was recorded using the Nicolet Genesis multi-channel data acquisition system at a sampling frequency of 5000 Hz.

The nAl-H_2O mixture was placed into a quartz sample cup or tube (10 mm O.D. × 30 mm), weighed, and installed in the closed vessel. For efficiency testing, the propellant ignition booster was replaced with a coiled nichrome wire, which was submerged into the reactant mixture surface. For each experiment, the chamber was sealed and purged with argon 2–3 times to remove excess air. The chamber was then brought to the desired initial pressure with a final fill of argon gas. The applied electrical load to nichrome coil varied from 50 to 75 Watts, depending on the chamber pressure and reactant mixture composition (i.e., particle size and ϕ). In general, mixtures with larger particle diameters required higher ignition energies.

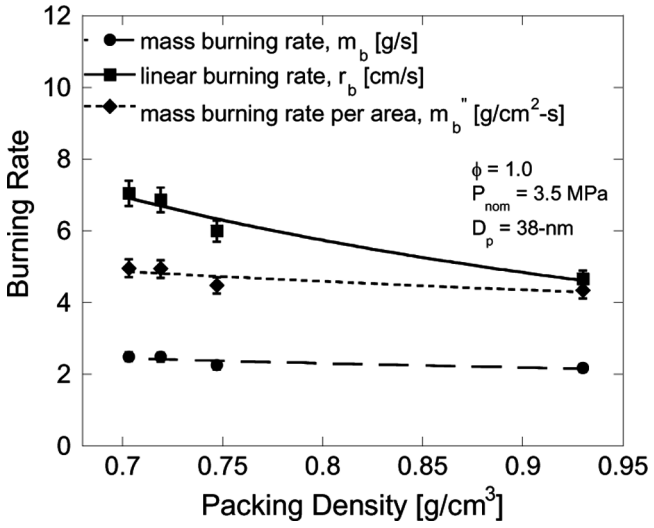

Figure 2 Mass and linear burning rates as a function of packing density.

To quantify the chemical efficiency, an Agilent micro gas chromatograph (MicroGC 3000) was used to measure the hydrogen concentration in the combustion chamber after each constant volume test. Calibration of the GC was accomplished by mixing hydrogen with argon and regulating the flows with calibrated mass flow controllers (Hastings 202C), thus relating the hydrogen chromatogram area to known hydrogen concentrations. The overall chemical efficiency, η_{chem}, was determined from

$$\eta_{\text{chem}} = \frac{[H_2]_{\text{meas}}}{[H_2]_{\text{theor}}}$$

where $[H_2]_{\text{meas}}$ is the hydrogen concentration from the GC measurement and $[H_2]_{\text{theor}}$ is the theoretical hydrogen produced based upon the overall ideal balanced chemical reaction,

$$2Al(s) + 3H_2O(1) + Ar \rightarrow Al_2O_3(s) + 3H_2 + Ar$$

Thus, high temperature dissociated species formed during the reactions were assumed to recombine to $Al_2O_3(s)$ and H_2 before GC analysis of the product gases. Therefore, any available H atoms are assumed to form molecular hydrogen. Also, since the amount of Poly-A was only a few percent in the overall mixture, its products were neglected. Figure 3 displays typical pressure-time profiles for 38 nm Al-H_2O mixtures reacting in the closed bomb. All mixtures had an equivalence ratio of 1.0 and an approximate total mass of 1.0 gm. The curves were offset by the respective initial pressure to easily compare peak pressure and pressurization rates. For elevated pressures, the initial pressurization rate appeared to be constant. However, for the atmospheric case, the pressurization rate was orders of magnitude slower. The measured maximum pressure is much less than the theoretical assuming a constant energy-volume reaction (NASA Chemical Equilibrium Applications Program-CEA, McBride and Gordon, 1996) as a result of heat loss to the surroundings.

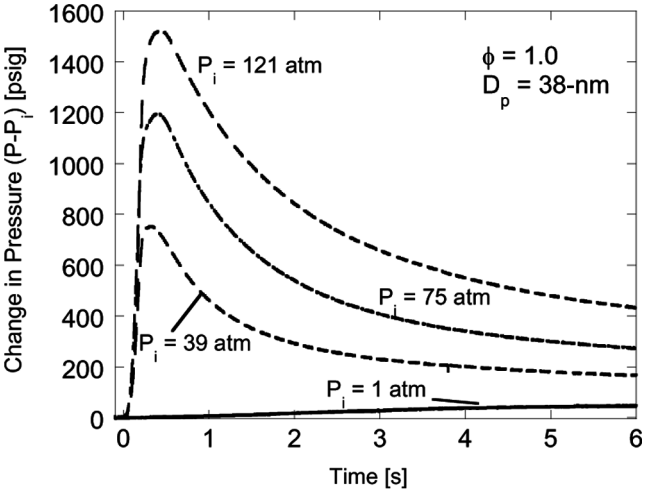

Figure 3 Pressure-time profiles of several closed bomb tests with various initial pressures and constant initial mixtures mass of ~1.0 gm.

RESULTS AND DISCUSSION

Figure 4 presents a series of video images showing the normal deflagration of stoichiometric 80 nm and 130 nm nAl and liquid water mixtures at $\sim$5.8 MPa. The onset of ignition is represented by t = 0 s. After approximately 0.10 s, normal deflagration was observed and the flame steadily propagated downward until the reactants were consumed. A visible flame appeared to be attached to the burning surface. Depending upon the mass-burning rate per area, a significant fraction of the alumina remained in the tube. The intense luminosity shown in Figure 4 indicates the emmision from the hot alumina above the propagation front. Videos of test strands using 38 nm particles do not glow as long as the 80 and 130 nm particles in the figure since a larger percentage of alumina is convectively carried out the top of the tube by the H_2 flow. The data from the digital video produced highly linear curves of position versus time, and hence, steady-state burning rates were achieved (Risha et al., 2007). The steadiness is also an indication of the uniformity in the packing density throughout the quartz tube.

Figure 5 shows the measured burning rates as a function of pressure for stoichiometric 38, 80, and 130 nm diameter nAl-water mixtures. For comparison, the results of Ivanov et al. (1994) using UFP Al and Poly-A are shown as well as our

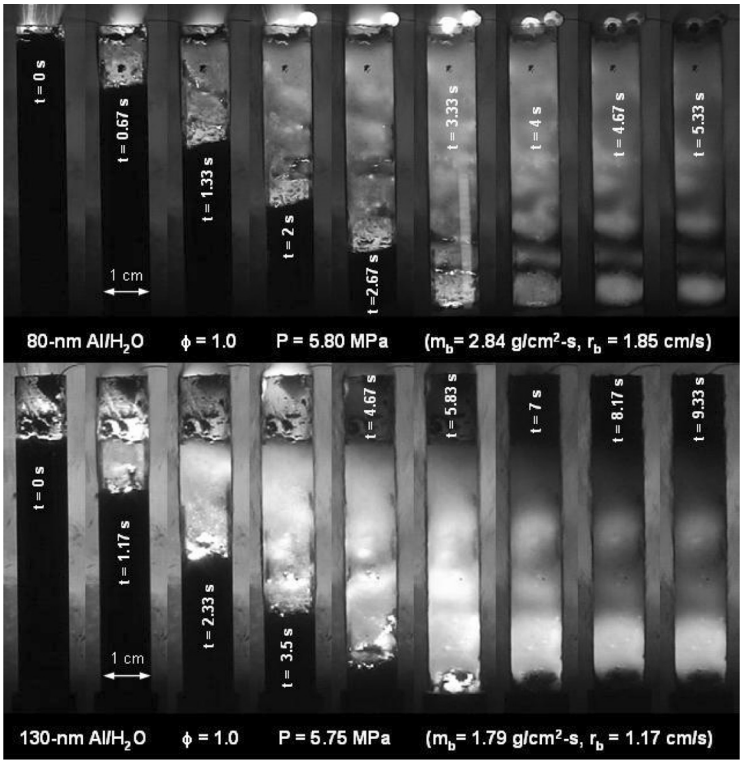

Figure 4 Captured images of the burning process of stoichiometric 80 and 130 nm diameter nAl/H_2O mixtures.

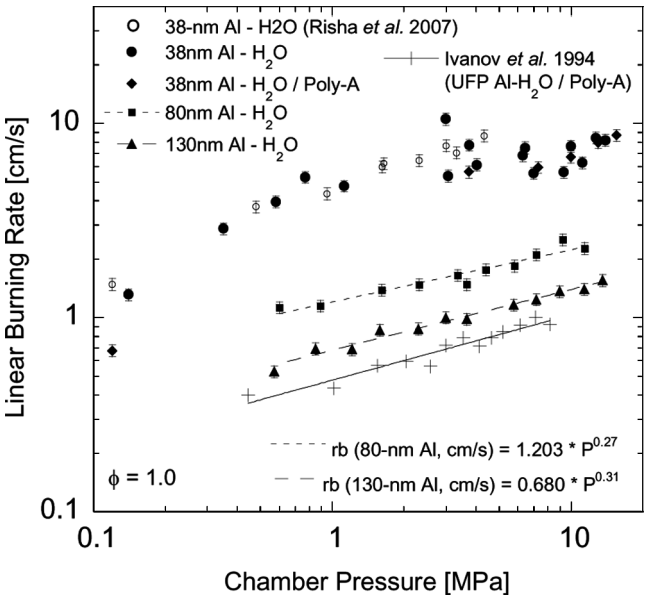

Figure 5 Effect of pressure on linear burning rate for a stoichiometric 38, 80, and 130 nm diameter nAl-H_2O and nAl-H_2O-Poly-A mixtures.

previous measurements for 38 nm Al particles below 4.35 MPa. The 80 nm, 130 nm, and UFP particles all exhibit constant pressure exponents in the burning rate formula over the pressure range considered, whereas the 38 nm particles begin to lose pressure dependence above approximately 3.5 MPa. For the pressures below 3.5 MPa, the 38 nm particles have a pressure exponent of $\sim$0.47 in the burning-rate formula (Risha et al., 2007). If the lowest pressure data are neglected ($<$0.3 MPa) since the mixture does not burn as smoothly at these pressures, the pressure exponent of the 38 nm particle mixtures is reduced to 0.44. The pressure exponents for the 80 and 130 nm particles were 0.27 and 0.31, respectively, over the entire pressure range considered.

The data from Ivanov et al. (1994), using the reported particle diameter of 1 μm (S.A. $= 18\,m^2/g$), yields a pressure exponent of 0.34, similar to that of the particles examined here. Based on the particle surface area data (Table 1), it is believed that the particles used by Ivanov et al. (1994) are actually much smaller, or perhaps a distribution with a large amount of finer particles. The low pressure exponents are advantageous for usage of these mixtures for propellants and gas generators and may be attributed to overall first-order heterogeneous reactions. As also shown in Figure 5, the burning rates were not affected by the addition of Poly-A to the reactant mixture.

The mass-burning rate per unit area (Figure 6) maintained the same trends as the linear burning rates, with the larger aluminum particles representing a single pressure exponent over the entire pressure range. The source of the discrepancy between the 38 nm particles and the larger diameter particles may be attributed to the high surface area and large oxide content of the particles. These two factors

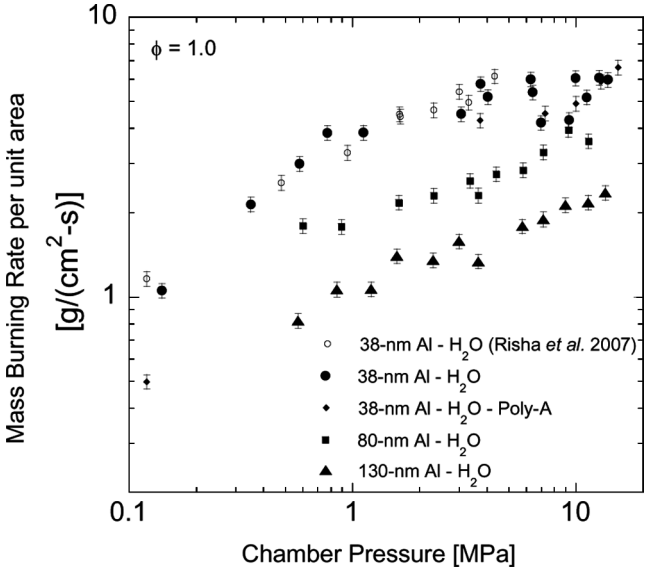

Figure 6 Effect of pressure on mass burning rate per area for a stoichiometric 38, 80, and 130 nm diameter nAl/H_2O and 38 nm diameter nAl-H_2O-Poly-A mixtures.

change the stoichiometric mixture consistency noticeably; thereby altering the packing density of the mixtures. Calculations show that the use of the 80 and 130 nm particles allow for packing densities greater than 90% of the theoretical maximum. In contrast, the packing densities of the 38 nm particle mixtures were generally between 40 and 50% of the theoretical maximum.

For the stoichiometric 38 nm particle mixtures, a large percentage of water is adsorbed onto the particle surface, yielding a "powder-like" consistency. The larger particles, which have much lower surface areas than the 38 nm particles, result in less water adsorbed onto the particle surface and more to fill voids between particles, thereby increasing packing density and creating stoichiometric mixtures with a "claylike" consistency. Figure 7 presents adiabatic flame temperatures for different particle size mixtures (McBride and Gordon, 1996) and illustrates how the presence of these voids, which are filled with argon gas during testing, may affect flame temperature as a function of pressure. The temperatures of the 130 nm particle mixtures are not affected by the presence of the argon. The 80 nm particle mixtures are only slightly affected by the argon since packing densities remain high and the volume of the voids is small. However, above approximately 1 MPa, the 38 nm particle mixtures begin to display a significant discrepancy in flame temperature between cases with and without argon consideration. Moreover, between 2 and 3 MPa, the flame temperature begins to decrease with pressure. Comparing Figure 7 with Figures 5 and 6, this onset of flame temperature reduction corresponds fairly well with the change in slope of burning rate for the 38 nm particle mixtures. The influence of the packing density on the mixture burning rates may also explain the increased scatter at higher pressures since the amount of void space, as well as individual void size, may be affected during the pressurization process.

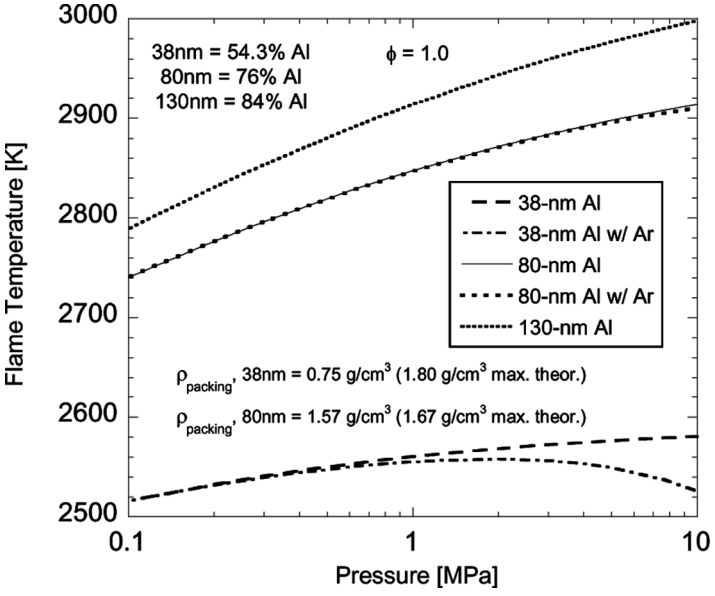

Figure 7 Equilibrium flame temperature of various mixtures of aluminum nanoparticles and liquid water.

Using the burning rate equations determined from experimental curve fits of the data, Figure 8 was created to further illustrate the effect of particle diameter on mass burning rate per unit area. Due to change in burning rate pressure dependency of the 38 nm particles, the burning rate equation was fitted to data below

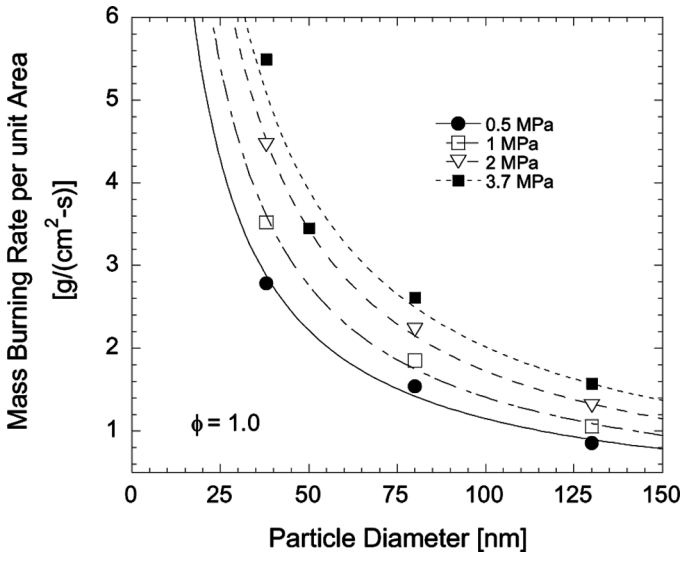

Figure 8 Mass burning rate per unit area as a function of aluminum particle diameter.

4 MPa. The figure clearly indicates that burning rate increases significantly with particle size. Although not shown on the plot, at all pressures considered, a diameter exponent of approximately D^{-1} is found by fitting the data to a single curve. This linear relationship of the burning rate with respect to particle diameter indicates the prevalence of a diffusion-controlled process for nanosized particles. Since only three diameters were considered at all pressures except at 2 MPa, where data for four diameters are reported, the uncertainty with this fit may be large.

Additionally, the 38 nm particles were produced by a different manufacturer than the 80 and 130 nm particles, resulting in differences in the oxide passivation layer such as thickness and morphology. Studies with more particle diameters are needed for a precise characterization of burning rate dependence on particle size, however at this time the available particle diameters from manufacturers is limited. Some burning rate data were obtained using 50 nm diameter particles from Technanogy as well, although available quantities did not allow for a complete study of pressure dependence. The 50 nm data point presented in Figure 8 is one of these results.

Increased scattering of the 50 nm diameter burning rate data and packing density was found, which may be a direct consequence of the surface area of the particles and mixing. Stoichiometric mixtures of these particles may lie on a precipice between mixtures which may be highly packed, and less dense powder-like mixtures. Larger, 5 micron particles were considered as well, however, ignition of these aluminum particles was not achieved for the pressures and type of ignition system used in this study. These results were anticipated since the specific surface area of micron-sized particles is relatively small, and thus, the mixture is less gelled. In addition, the rate of energy delivery from the igniter was not rapid enough to heat up the micron-sized aluminum to its ignition temperature, and consequently, much of the energy from the igniter was expended to vaporize the water without reacting with the aluminum.

Another contributing factor is that micron-sized aluminum particles need much higher temperatures ($\sim$2000 K) than nAl ($\sim$900 K) to ignite (Parr et al., 1999; Trunov et al., 2005) even though having larger active aluminum content. In contrast, nAl particles have the ability to absorb large amounts of water on the surface (thus gelling and improving the mixedness of the mixture) as well as to heat up quicker (smaller heat capacity).

The chemical efficiency, η_{chem}, is an important parameter for characterizing the nAl-mixtures. Burning rates by themselves may not be adequate since they do not necessary quantify the extent of reaction. In these simple two-component aluminum-water mixtures, the number of combustion products is small and they are relatively easy to quantify. For stoichiometric proportions, the only product species that exist, neglecting dissociation, are alumina and hydrogen gas. Thus, the quantity of hydrogen gas is a direct measurement of the completeness of the reaction. Figure 9 shows the product species mole fractions and adiabatic flame temperature as functions of equivalence ratio at a pressure of 3.5 MPa.

The solid amorphous aluminum oxide, Al_2O_3(a), is present until around $\phi = 0.6$, which is a result of the adiabatic flame temperature being lower than the melting temperature of alumina. When the flame temperature exceeds the melting point of Al_2O_3 ($\phi \sim 0.7$), the solid aluminum oxide changes phase and liquid Al_2O_3 becomes the dominant product. For fuel rich conditions, aluminum was present and steadily increased until $\phi \sim 1.2$, where the rate of its increase slowed.

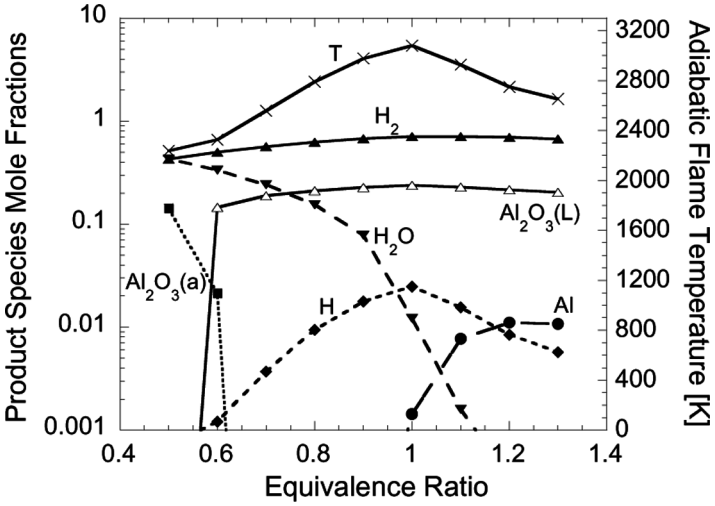

Figure 9 Mole fractions of product species as a function of equivalence ratio for 38 nm diameter nAl-H_2O at P = 3.65 MPa.

As expected, at $\phi = 1$, the atomic hydrogen is at a maximum and decreases for both fuel-lean and fuel-rich conditions indicating that maximum dissociation occurs at the peak temperature. Using the simple balance equation for aluminum-water, 75% (by vol) of hydrogen gas is produced for 1 mole of aluminum. The equilibrium calculations, which include dissociation, indicate a slightly lower hydrogen production of approximately 71% (by vol). The only other major species is atomic H (~2.5%) due to hydrogen dissociation.

Figure 10 shows the dependence of chemical efficiency on pressure for 38 nm particle mixtures. Over the entire range considered, η_{chem} was nearly independent of pressure for nAl-H_2O and nAl-H_2O-Poly-A mixtures. The efficiency for the Poly-A mixtures with 38 nm particles were greater than 75% for all pressures studied and as high as 91%. The mixtures without Poly-A exhibited efficiencies between 87 and 98%. The average uncertainty in these combustion efficiencies was 5–6%. Table 2 contains the chemical efficiencies for fuel-lean conditions ($\phi = 0.67$) for the 38 nm nAl-H_2O mixtures. The increased η_{chem} with pressure may be caused by various phenomena such as increased vaporization temperature and slightly better interaction between the fuel and oxidizer.

Depending upon the stoichiometry and particle diameter, the condensed-phase products varied in structure and color. For lean mixtures, low-initial pressure, and large diameter particles, the solid products were grayish and formed large agglomerates. In contrast, for high pressures and large particle diameters, the condensed-phase products appeared whiter and consisted of very fine powder-like particles. It was also found that the particle diameter, as well as the sample preparation, had a strong effect on the amount of hydrogen generated during combustion, with values as low as ~28% (by vol) for unconfined 130 nm particles to nearly 100% (by vol) for 38 nm particles. This increase is expected since complete combustion

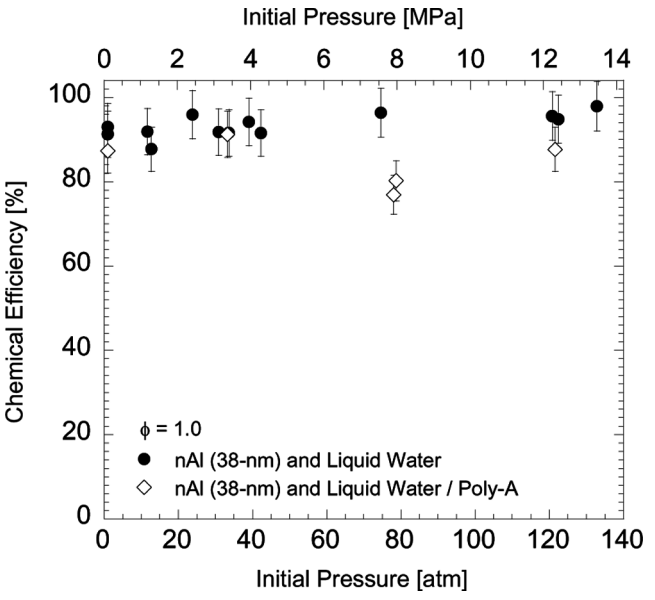

Figure 10 Chemical efficiency for 38 nm nAl-H_2O and nAl-H_2O-Poly-A mixtures at various pressures.

has a greater chance with smaller particles due to the reduced heat loss to the surroundings for faster burning particles.

Furthermore, confinement (i.e., packing density) was found to play an important role in the combustion efficiency, particularly with the large particles investigated. The majority of testing was completed by placing the particles unconfined in a small quartz crucible. However, some samples were packed into 10 mm O.D. quartz tubes, such as those used for burning rate measurements. When using the 38 nm particles, efficiencies were found to be unaffected by the sample preparation; however, when using the 80 and 130 nm particles, efficiency increased significantly when packed into the quartz tubes. In some cases efficiencies of 80–85% were found with the 130 nm particles. Due to the much longer burning times of the larger particles the confinement reduced the amount of heat loss to the surroundings, which enabled the particles to burn to near completion before quenching.

Ignition in the closed bomb with the nichrome wire proved to be difficult and unreliable with larger particles. Occasionally, ignition was observed but efficiencies were quite low. Analysis of the reaction products revealed a gray, dried-out product, and much of the chamber walls were coated with water. Since particles used in these

Table 2 Chemical efficiency for nAl-H_2O mixtures at $\phi = 0.67$

P [atm]	Chemical efficiency [±6%]
39.5	79.1
68.9	86.7
122.3	99.5

studies have a size distribution associated with their nominal diameter, it is believed that the observed ignition was due to the reaction of small diameter particles within this size distribution, which are more reactive. The resulting reaction was exothermic enough to vaporize the liquid water, which then condensed on the walls of the closed bomb, without reacting with the majority of the Al present as larger particles. Overall, the larger particles required significantly more ignition energy to produce highly efficient reactions than the 38 nm particles. Chemical efficiency of 80 nm particles ($\sim$80%) was not affected by the presence of Poly-A in the oxidizer and was higher than published data by Shafirovich et al. (2006), which was approximately 50%. This discrepancy may be attributed to mixing techniques, sample loading (i.e., confinement in tube) or pressure since Shafirovich et al. (2006) results were at 1 atm.

CONCLUSIONS

The combustion and chemical efficiency of nano-aluminum (nAl) and liquid water has been characterized for nAl-H_2O and nAl-H_2O-poly(acrylamide-co-acrylic acid) mixtures for a broad range of pressure, mixture composition, and particle size. Several parameters can affect the aluminum-water reaction in terms of burning rate or chemical efficiency such as particle diameter, active aluminum content, and oxide layer thickness.

Linear and mass burning rates of 38 nm mixtures were found to obey a $\sim P^{0.5}$ burning rate power law up to 3.5 MPa. Beyond 3.5 MPa, the burning rate became independent of pressure. This trend is explained by the presence of significant void space in the mixture, which is occupied by argon during testing, reducing flame temperatures at high pressure. Larger particles exhibit lower specific surface areas, and higher aluminum content, altering the stoichiometric mixture consistency and reducing void space to an energetically insignificant amount when filled with Ar. Mixtures of 80 and 130 nm particles exhibited burning rate pressure exponents of 0.27 and 0.31, respectively, over the entire range of pressures considered. These exponents compare extremely well to the data of Ivanov et al. (1994), who used mixtures of UFP aluminum with liquid water and a 3% (by mass) addition of poly(acrylamide-co-acrylic acid) gelling agent. Poly-A was also added to mixtures of 38 and 80 nm Al particles and water in this study without significantly affecting the burning rates or chemical efficiencies of the mixtures.

Linear and mass burning rates, as well as chemical combustion efficiencies were observed to depend on particle diameter. Based on a limited data set of particle diameters, the results indicate a D^{-1} burning rate dependence on particle diameter, which indicates a diffusion controlled combustion process. More data are required from a larger number and range of particle diameters in order to solidify the burning rate dependence. Regardless, it is clear that reducing particle size may significantly increase burning rates. At 1 MPa, linear burning rate increased $\sim$7 times, and mass burning rate per unit area increased $\sim$3.3 times by reducing particle diameter from 130 to 38 nm.

At all pressures considered, combustion of 38-nm particle mixtures achieved greater than 85% of maximum theoretical chemical conversion. In some cases, efficiencies greater than 95% were found. These conversion efficiencies were easily reproduced regardless of sample packing density and orientation. Larger particles produced

proportionally lower efficiencies, with 130 nm particles consistently producing the lowest efficiencies of the three primary particle sizes studied (i.e., 38, 80, and 130 nm). Larger particle mixture chemical efficiencies also exhibited a strong dependence on the sample orientation (i.e., packing density) and input ignition energy. Unconfined mixtures produced considerably lower efficiencies than mixtures confined and packed into a small tube due to increased energy loss to the surroundings.

REFERENCES

Basilev, A.V., Gorbubunov, V.V., and Shidlovskii, A.A. (1970) Effect of some additives on the critical diameter and the rate of combustion of mixtures of aluminum with gelatinized water. *Khimiya i Khimicheskaya Tekhnologiya* (*USSR*), **13**(3), 318–321.

Bucher, P., Yetter, R.A., Dryer, F.L., Parr, T.P., and Hanson-Parr, D.M. (1998) PLIF species and radiometric temperature measurements of aluminum particle combustion in O_2, CO_2 and N_2O oxidizers, and comparison with model calculations. *Proc. Combust. Instit.*, **27**, 2421–2429.

Foote, J.P., Lineberry, J.T., Thompson, B.R., and Winkelman, B.C. (1996) Investigation of aluminum particle combustion for underwater applications. *AIAA Paper*, 1996–2086, 32nd AIAA/ASME/SAE/ASEE Joint Propulsion Conference, Orlando, FL.

Glassman, I. (1996) *Combustion*, 3rd ed., Orlando, FL, Academic Press, Chap. 9.

Goroshin, S., Fomenko, I., and Lee, J.H.S. (1996) Burning velocities in fuel-rich aluminum dust clouds. *Proc. Combust. Instit.*, **26**, 1961–1967.

Greiner, L. (1960) Selection of high-performance propellants for torpedoes. *ARS J.*, **30**, 1161–1163.

Greiner, L. (1962) Underwater Missile Propulsion. Compass Publications Inc., Arlington, VA.

Il'in, A.Q.P., Gromov, A.A., Vereshchagin, V.I., Popenko, E.M., Surgin, V.A., and Lehn, H. (2001) Combustion of ultrafine aluminum powder in air. *Combust. Explos. Shock Waves*, **37**(6), 664–668.

Ingenito, A. and Bruno, C. (2004) Using aluminum for space propulsion. *J. Propul. Power*, **20**(6), 1056–1063.

Ivanov, V.G., Gavrilyuk, O.V., Glazkov, O.V., and Safronov, M.N. (2000) Specific features of the reaction between ultrafine aluminum and water in a combustion regime. *Combust. Explos. Shock Waves*, **36**(2), 213–219.

Ivanov, V., Ivanov, V.G., Gavriluk, O.V., and Glazkov, O.V. (1995) Combustion of electro-exploded aluminum in liquid media. *JANNAF Propulsion Meeting*, Tampa, FL.

Ivanov, V.G., Leonov, S.N., Savinov, G.L., Gavrilyuk, O.V., and Glazkov, O.V. (1994) Combustion mixtures of ultradisperse aluminum and gel-like water. *Combust. Explos. Shock Waves*, **30**(4), 569–570.

Lee, W.M. (1993) Aluminum Powder/Water Reaction Ignited by Electrical Pulsed Power. Naval Surface Warfare Center, Report Number AD-A269223.

McBride, B.J. and Gordon, S. (1996) Computer Program for Calculation of Complex Chemical Equilibrium Compositions and Applications. NASA, Reference Publication 1311.

Miller, T.F. and Herr, J.D. (2004) Green Rocket Propulsion by Reaction of Al and Mg Powders and Water. *AIAA Paper*, 2004–4037, 40th AIAA/ASME/SAE/ASEE Joint Propulsion Conference and Exhibit, Fort Lauderdale, FL.

Parr, T.P., Hanson-Parr, D.M., and Yetter, R.A. (1999) Flame Structure Studies of Ultra-Fine Aluminum and Fluorine Containing Propellants. *36th JANNAF Combustion Subcommittee Meeting*, Cocoa Beach, FL.

Rasor, O. (1942) Power Plant. U.S. Patent 2,289,682.

Risha, G.A., Huang, Y., Yang, V., Yetter, R.A., Son, S.F., and Tappan, B.C. (2006) Combustion of Aluminum Particles with Steam and Liquid Water. *AIAA*, 2006–1154, 44th AIAA Aerospace Sciences Meeting and Exhibit, Reno, NV.

Risha, G.A., Huang, Y., Yetter, R.A., and Yang, V. (2005) Experimental Investigation of Aluminum Particle Dust Cloud Combustion under Various Oxidizing Environments. *AIAA Paper*, 2005-0739, 43rd AIAA Aerospace Sciences Meeting and Exhibit, Reno, NV.

Risha, G.A., Son, S.F., Yetter, R.A., Yang, V., and Tappan, B.C. (2007) Combustion of nano-aluminum and liquid water. *Proc. Combust. Instit.*, **31**, 2029–2036.

Shafirovich, E., Dialov, V., and Varma, A. (2006) Combustion of novel chemical mixtures for hydrogen generation. *Combust. Flame*, **144**, 415–418.

Smith, I.E. (1972) Hydrogen generation by means of the aluminum/water reaction. *J. Hydronaut.*, **6**(2), 106–109.

Tao, W.C., Frank, A.M., Clements, R.E., and Shepherd, J.E. (1990) Aluminum metal combustion in water by high speed microphotography. *International Symposium on Optical and Optoelectronic Applied Science and Engineering Exhibit*, **1346**, 300–310.

Trunov, M.A., Schoenitz, M., and Dreizin, E.L. (2005) Ignition of aluminum powders under different experimental conditions. *Propel. Explos. Pyrotech.*, **30**(1), 36–43.

Williams, F.A. (1985) *Combustion Theory*, Redwood City, CA, Addison Wesley.

Williams, F.A. (1997) Some aspects of metal particle combustion. In: Dryer, F.L. and Sawyer, R.F. (Eds.) Physical and Chemical Aspects of Combustion: A Tribute to Irvin Glassman, Gordon and Breach, Netherlands, Chap. 11, pp. 267.

Yetter, R.A. and Dryer, F.L. (2001) Metal particle combustion and classification. In: Ross, H.D. (Ed.) *Microgravity Combustion*, Academic Press, San Diego, CA, Chap. 6.